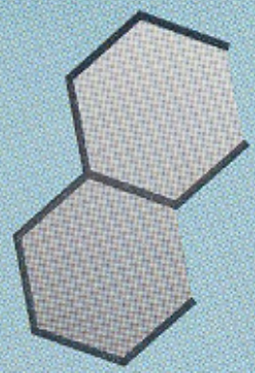

Carbon'02 in Beijing

An International Conference on Carbon
15-19 September 2002 Beijing, CHINA

SHANXI CHUNQIU AUDIO-VISUAL PRESS
ISBN 7-900362-03-7/G.03

CARBON '02

An International Conference on Carbon

September 15-20, 2002 Beijing, China

"CARBON 2002" – An International Conference on Carbon (15-19 September 2002, Beijing, CHINA)
CD-ROM Proceedings (SHANXI CHUNQIU AUDIO – VISUAL PRESS. ISBN 7-900362-03-7/G.03)

SURFACE AND INTERFACE SPIN RELAXATION IN GRAPHITE, NANOGRAPHITE AND THEIR INTERCALATION COMPOUNDS

A.M. Ziatdinov*
Institute of Chemistry, Far Eastern Branch of the Russian Academy of Sciences.
159, Prosp. 100-letiya, 690022 Vladivostok, Russia

Abstract – In all previous investigations of conduction ESR (CESR) phenomenon in graphite and its intercalation compounds at the analysis of the resonance line shape the surface and interface spin relaxation effects were neglected. We have studied the dependences of lineshape, linewidth and intensity of CESR signal in these materials on sample dimensions and experimental conditions and have shown the presence of the strong surface or/and interface spin relaxation effects for cunduction carriers. The some data concerning to the CESR phenomenon in nanographites and their intercalation compounds with nitric acid are also presented and discussed.

Keywords: **A**. graphite, intercalation compounds; **B**. electron paramagnetic resonance; **D**. electronic and magnetic properties.

1. INTRODUCTION

The method of conduction ESR (CESR) has been actively used in studies of graphite and graphite intercalation compounds (GICs) for determining the kinetic parameters of the spin carriers from an analysis of the Conduction ESR (CESR) line shape [1-11]. For a long time the analysis of the CESR line shape for the graphite itself [1,2,11-14] and its intercalation compounds [3-10] was carried out using the well-known theory of Dyson [15] and Kaplan [16] not including the surface spin relaxation of current carriers by the standard procedures of Feher and Kip [17], Kodera [18], and Pifer and Magno [19]. However, in a strict sense, Dyson's theory [15] of the CESR is applicable only for infinite metal plates of arbitrary thickness with isotropic conductivity and a single carrier type. Although experiments have shown the validity of using this theory for analyzing the CESR line shape in metal plates with finite dimensions, its applicability to the case of graphite and GICs with large anisotropy of skin depths, as well as anisotropy of carrier diffusion, is not obvious. First, it was pointed out by Müller *et al*. [20]. Later, Saint Jean *et al*. [8] and Blinowski *et al*. [21] have studied this problem mathematically strictly using the Maxwell equations. To obtain the correct CESR line shape analysis in the case of anisotropic conductors, they have extended the Dyson theory [15] by taking into account the anisotropy of conductivity and diffusion. Herewith, authors, as well as all preceding researchers, implied that in graphite and GICs it is possible to neglect the surface spin relaxation effects.

In this paper the experimental results for the dependence of CESR signal parameters in highly oriented pyrolitic graphite (HOPG) and in GICs with nitric acid on sample dimensions and experimental conditions are presented. The analysis of this results uniquely points to the presence of the strong surface and interface spin relaxation effects in samples investigated. The some data concerning to the CESR phenomenon in nanographites and in their intercalation compounds with nitric acid are also presented and discussed.

*Corresponding author. Fax: +7-4232-311889; e-mail address: albert_ziatdinov@mail.primorye.ru

2. EXPERIMENTAL

CESR measurements were carried using an X-band E-line spectrometer in a rectangular cavity with TE_{102} mode. The constant magnetic field ($\boldsymbol{H}_0$) modulation frequency and amplitude were 2.5 kHz and 0.1 mT, respectively.

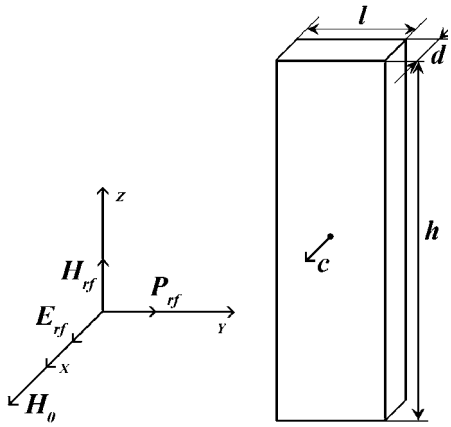

Fig. 1. The orientation of the HOPG slab with respect to the external magnetic field $\boldsymbol{H}_0$ and the cavity axis (*X*, *Y* and *Z*). $\boldsymbol{H}_{rf}$, $\boldsymbol{E}_{rf}$ and $\boldsymbol{P}_{rf}$ are the magnetic and electric components of the radio-frequency field, and the Pointing vector in an unloaded rectangular cavity, respectively.

All graphite plates for the experiments were cut from a single sample of HOPG and they were in the shape of rectangular parallepipeds with the dimensions width (l)×height (h)×thickness (d), where $h \times l$ is the area of the basal face (Fig. 1).

The study of dependences of graphite CESR lineshape on sample dimensions were carried out on HOPG plates with dimensions:: $l \times 0.355 \times 0.072$ cm^3. The accuracy in the determination of the sample dimensions was ~5×10^{-4} cm.

The plates were fastened by the basal face on the planar surface of the goniometer rod, which was cut along its axis so that two of the lateral faces of the plate ($h \times d$) were parallel to the given axis (and $\boldsymbol{H}_{rf}$). With the plates fastened

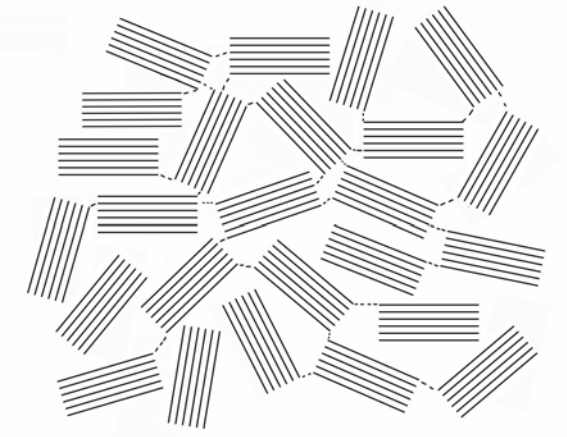

Fig. 2. The micrograpitic model structure of activated carbon fibers. The broken line denotes the sp^3 linkage.

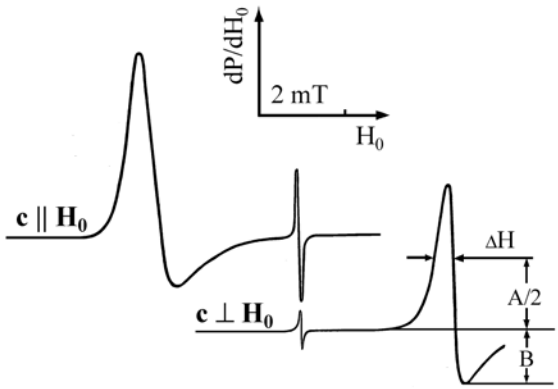

Fig. 3. The first derivative of CESR signal in HOPG slab with the dimensions: 0,364×0,355×0,072 cm^3. The narrow symmetrical line corresponds to the Mn^{2+} EPR signal in the standart sample ZnS:Mn^{2+}. $\boldsymbol{c} \perp \boldsymbol{H}_{rf}$; ν=9,52 HHz . T=300 K.

this way, their ***c***-axis lay in a horizontal plane. The samples were placed in the antinode of $\boldsymbol{H}_{rf}$.

Synthesis of the 2-nd stage GICs with nitric acid, $C_{10}HNO_3$, was carried out in liquid nitric acid with density ρ~1.565 g/cm^3 on HOPG plates with dimensions: l×0.5×0.01 cm^3. The stage structure of the GICs was determined by X-ray diffractometer.

The *in situ* CESR study of graphite intercalation by nitric acid were carried out on HOPG plates with dimensions: 0.4×0.04×0.02 cm^3 and 0.4×0.045×0.03 cm^3. The HOPG samples were held in quartz tube connected via a valve to the reservoir with intercalate (liquid HNO_3 with density $\rho \cong$ 1.565 g/cm^3). Nitric acid vapours penetrated into the knee of reactor with the graphite sample through the hole with the size $\approx 8\times10^{-3}$ cm^2 in the fluoroplastic diaphragm. Prior to the experiment, the system was evacuated to eliminate air and water. During the measurements, $\boldsymbol{H}_0$ was applied along the graphite ***c***-axis.

According to the data of four-probe method, at 300 K the ***c***-axis conductivity (σ_c) of HOPG plate used is equal to (7.7±0.8) S/cm. In the X-band experiment the value of skin depth δ_c~0.02 cm corresponds to this conductivity, i. e. in CESR experiment of *in situ* graphite intercalation by nitric acid the whole volume of the HOPG plate investigated was available for the CESR studies.

The investigated samples of ACF were obtained commercially. The X-ray-diffraction profiles of ACFs were obtained by Simens SMART CCD instrument with a Mo target (50 kV, 30 mA). In Fig. 2, the micrograpitic model structure of ACF used in experiments is presented.

The temperature studies of CESR spectra of the samples investigated were carried out in the temperature range from 4,2 K to 350 K. The temperature was maintained and measured with an accuracy of ~0.1 K/h and ~0.5 K, respectively.

3. RESULTS

3.1 *Graphite.*

The CESR spectrum of all HOPG plates investigated consists of a single asymmetric line (Fig. 3) determined by the Dyson-Kaplan mechanism [15, 16]. The spectrum is axial with respect to the ***c***-axis and the principal values of *g*-factor determined by Feher-Kip [17] nomograms or those of Kodera [18] are equal to g_c=2.0474±0.0002 and g_a=2.0029±0.0002 for $\boldsymbol{H}_0 \| \boldsymbol{c}$ and $\boldsymbol{H}_0 \perp \boldsymbol{c}$, respectively.

For the "thick" plates (d>0.045 cm) the dependence of asymmetry parameter, A/B, of the first derivative of CESR absorption line, which is equal to the ratio of the peak intensity of the more intense wing, A, to that of the less intense wing, B, vs. l has three-peak form (Fig. 4). In the interval $l_{1m} < l < l_{2m}$, where l_{1m} (l_{2m}) is the coordinate of the first (second) peak - in the direction of l increase, the line has an inverted line-shape phase – the A peak is located at a higher magnetic field than the B peak. At l_{1m} and l_{2m} the line is symmetrical about the A peak, and the value of A/B is a maximum. The third, diffuse maximum is not associated with the change of phase of the line shape.

At $l \to 0$ the experimental values of CESR linewidth tends to the infinity (Fig. 5).

For all orientations of $\boldsymbol{H}_0$ relative to the ***c***-axis the ΔH increases first with decreasing temperature, forms a distinct peak at about 20 K and then falls off leftward (Fig. 6). The *g*–factor for $\boldsymbol{H}_0 \perp \boldsymbol{c}$ almost independent of temperature (Fig. 7). With the $\boldsymbol{H}_0 \| \boldsymbol{c}$, the *g*-value increases first with decreasing temperature, but it forms a distinct peak at about 20 K in a manner similar to that of the $\Delta H(T)$ (Fig. 7).

3.2 *Graphite intercalation by HNO_3.*

After outflow of certain time (so-called "induction" time depending on sample size and experimental conditions) after the injection of HNO_3 gas into the part of the reactor with the HOPG plate, the CESR signal of graphite begins to transform and decrease in intensity until it fully disappears after ~3 hours (Fig. 8). Simultaneously a new signal with g_c*=2.0019±0.0002, and g_a*=2.0030±0.0002 appears in the spectrum (Fig. 9), where g_i* (i = a, c) value is determined by the H_0 value at the point of intersection of the first derivative of CESR absorption line and the base line.

The linewidth (the intensity), ΔH ($I=(A+B)\times\Delta H^2$), of the graphite CESR signal increases (decreases) vs. exposure time, τ, monotonously (Fig. 8 and 10). In an initial HOPG sample, which was used in experiment on intercalation, the CESR lineshape is 'normal' in the sense that the maximum peak height occurs at the lower magnetic fields. At the beginning of reaction the A/B ratio of graphite signal increases, but it is still 'normal' reaching a maximum value of A/B>8. Later, upon further exposure in the intercalate atmosphere, the A/B ratio becomes 'reversed' (maximum peak height, A, occurs at higher magnetic fields than the peak B), and its magnitude

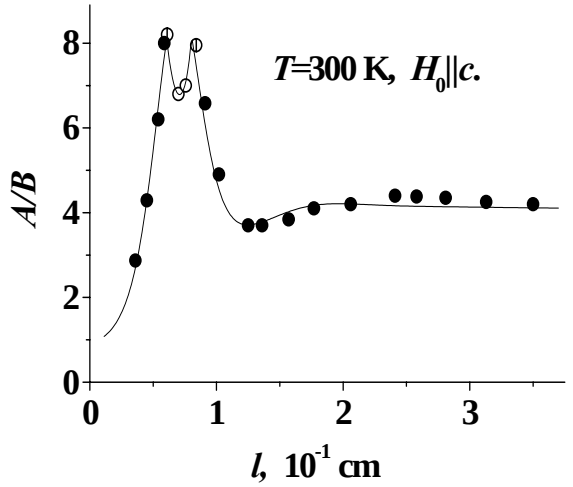

Fig. 4. The experimental (dots) and the theoretical (solid line) values of CESR line shape asymmetry parameter, *A/B*, in graphite vs. sample width *l*. The shaded and open dots are referred to the normal and 'reversed' lineshape, respectively; half-shaded dot corresponds to the lineshape with symmetric phase with respect to the *A* peak. G_a=200 cm^{-1}, R_a=2.35, R_c=6, T_2=1.16×10^{-8} s. $R_i=(T_{Di}/T_2)^{1/2}$ (T_{Di} (i=a, c) is the time of spin diffusion across the skin-depth δ_i (i=c, a) governed by the σ_i – conductivity (i=c, a), and T_2 is the intrinsic spin-relaxation time), δ_c=0.02 cm. The X-band.

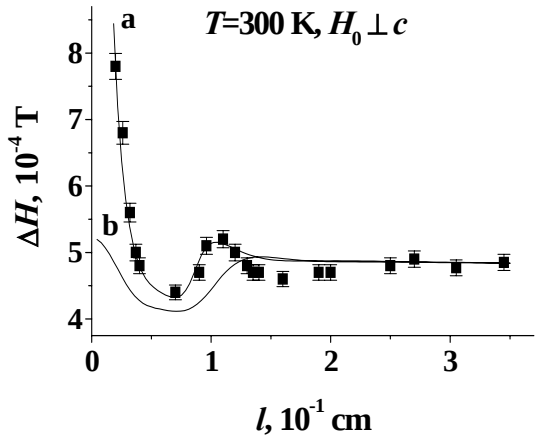

Fig. 5. The experimental (dots) and the theoretical (solid lines) values of linewidth, Δ*H*, in graphite vs. sample width *l*. The curve a (b) corresponds to the value of Dyson [15] surface spin relaxation parameter G_a=180 (0) cm^{-1}. R_a=2.5, R_c=6, T_2=1.38×10^{-8} s. $R_i=(T_{Di}/T_2)^{1/2}$ (T_{Di} (i=a, c) is the time of spin diffusion across the skin-depth δ_i (i=c, a) governed by the σ_i – conductivity (i=c, a), and T_2 is the intrinsic spin-relaxation time), δ_c=0.02 cm. The X-band.

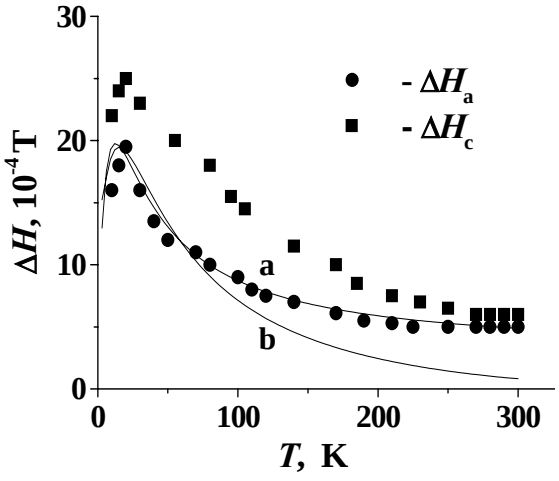

Fig. 6. The experimental (dots) and theoretical (lines) values of CESR linewidth, Δ*H*, in HOPG plates vs. temperature *T*. The theoretical curves (a) and (b) were calculated using the Exp. (2) with constant (= 4.4×10^{-4} T) and determined by the Exp. 4 values of linewidth (the intrinsic conduction electron spin relaxation time), respectively, and Dyson [15] surface spin relaxation parameter G_a=180 cm^{-1}. The X-band.

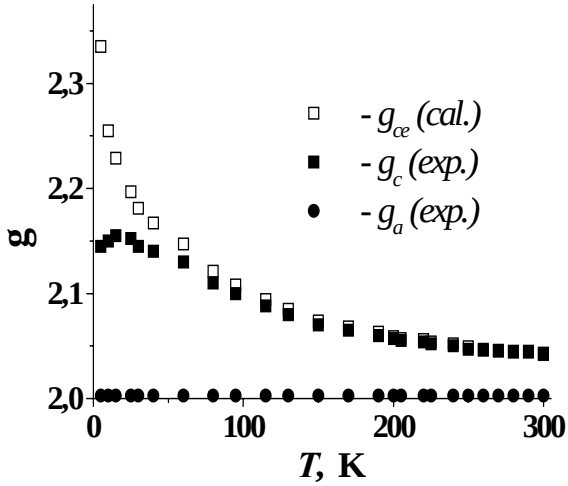

Fig. 7. Experimental (solid dots) and calculated (open dots) values *g*-factor for CESR signal in HOPG vs. temperature. The g_{ce}-values were extracted from the expression: $\Delta g_c(exp)=\Delta g_{ce}(\chi_e/\chi_e+\chi_s)+\Delta g_{cs}(\chi_s/\chi_e+\chi_s)$, where Δg_{ce} and Δg_{cs} are the values of *g*-shifts for the conduction electrons and the localized spins, respectively, both at $\boldsymbol{H}_0\|\boldsymbol{c}$. The X-band.

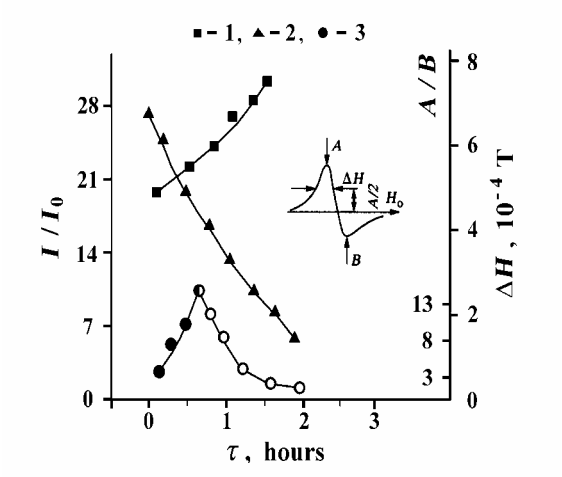

Fig. 8. CESR lineshape parameters for non-intercalated parts of the narrow (l~$2\delta_c$) HOPG plate vs. exposure time, τ, in HNO_3 atmosphere. 1, 2 and 3 correspond to ΔH, A/B and I/I_0, respectively (I=(A+B)×ΔH^2; I_0 is the intensity of the Mn^{2+} ESR signal of the standard sample: ZnS:Mn^{2+}). The shaded and open dots are referred to the 'normal' and 'reversed' lineshape, respectively; half-shaded dot corresponds to the lineshape with symmetric phase with respect to the A peak. The X-band; T=300 K. The lines are only a guide to the eye.

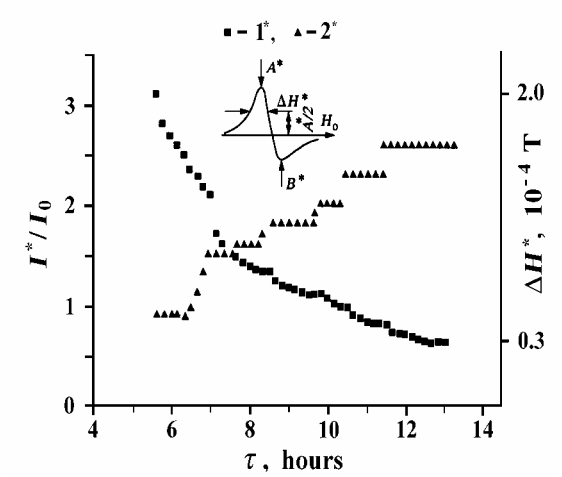

Figure 9. CESR lineshape parameters for intercalated parts of the narrow (l~$2\delta_c$) HOPG plate vs. exposure time, τ, in HNO_3 atmosphere. 1*, 2* and 3* correspond to ΔH*, A*/B* and I*/I_0, respectively (I* = (A*+B*)×(ΔH*)^2; I_0 is the intensity of the Mn^{2+} ESR signal of the standard sample: ZnS:Mn^{2+}. The X-band; T=300 K.

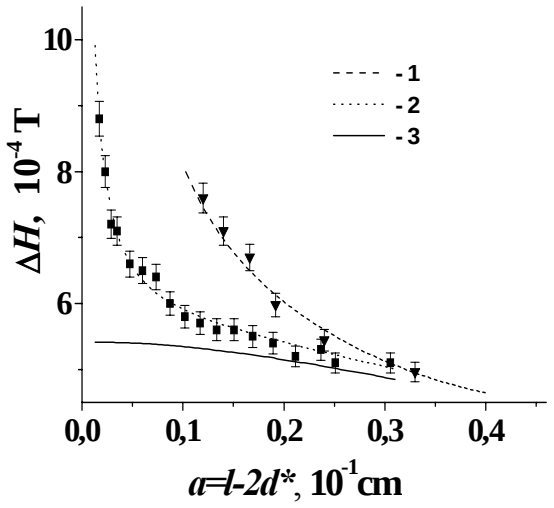

Fig. 10.The experimental (dots) and theoretical (lines) values of CESR linewidth, ΔH, vs. thickness, a, of the non-intercalated (by HNO_3) part of HOPG plate (for two different samples). 1: G_a=10 cm^{-1}, T_2=1.15×10^{-8} s, δ_c=0.013 cm; 2: G_a=1 cm^{-1}, T_2=1.3×10^{-8} s, δ_c=0.02 cm; 3: G_a=0, T_2=1×10^{-8} s, δ_c=0.02 cm. $\boldsymbol{H}_0\|\boldsymbol{c}$, T=300 K.

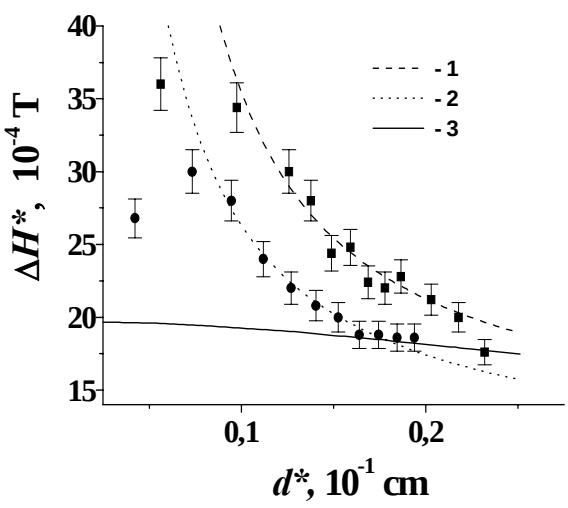

Fig. 11.The experimental (dots) and theoretical (lines) values of CESR linewidth, ΔH*, vs. thickness, d*, of the intercalated (by HNO_3) part of HOPG plate (for two different samples). 1: G^*_a=180 cm^{-1}, T^*_2=0.38×10^{-8} s, δ_c^*=0.025 cm; 2: G^*_a=70 cm^{-1}, T^*_2= 0.45×10^{-8} s, δ_c^*=0.025 cm; 3: G_a=0, T_2=0.35×10^{-8} s, δ_c=0.025 cm. $\boldsymbol{H}_0\|\boldsymbol{c}$, T=300 K.

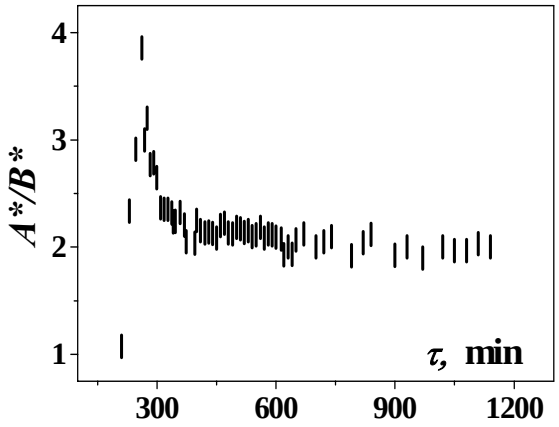

Fig. 12. The CESR lineshape asymmetry parameter, A^*/B^*, of the intercalated part of HOPG plate vs. exposure time, τ, in HNO_3 atmosphere. The X-band; T=300 K.

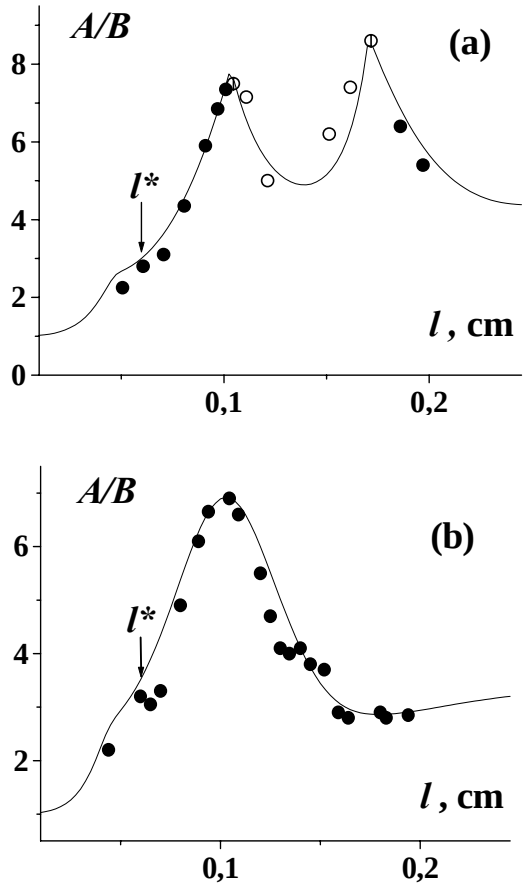

Fig. 13. The experimental (dots) and the theoretical (solid line) values of the asymmetry parameter, *A/B*, in $C_{10}HNO_3$ plates vs. l at $T>T_c$ (a) and $T<T_c$ (b). At $T>T_c$ [$T<T_c$] G_a, R_a, T_2 and δ_c are equal to 23 cm^{-1} [$(5.4+270\cdot\exp(-l/l_0))$ cm^{-1}, where l_0=0.025 cm], 1[1.5], 2.8[0.8]×10^{-7} s and 4.3[3.7]×10^{-2} cm, respectively. The shaded, open and half-shaded dots are referred to the 'normal', 'reversed' and symmetric lineshapes with respect to the *A* peak, respectively. The X-band.

decreases down to value less than 2.55 ; the *A/B* maximum corresponds to the moment when the 'reversal' of CESR lineshape takes place (Fig. 8). The g_i (i = a, c) value of graphite CESR signal does not change up to its disappearance.

For the CESR signal with g_i* both the intensity, $I^*=(A^*+B^*)\times(\Delta H^*)^2$, and linewidth, ΔH^*, dependences versus exposure time take a well-marked step-wise form (Fig. 9). At the moment of first observation the A^*/B^* value of this signal ~1, then the value of asymmetry parameter increases up to 3.8, forms a distinct peak and decreases up to 2.2 to the end of reaction (Fig. 12). The g_i*-values of this signal remain constant up to the end of intercalation.

3.3 *Graphite intercalation compounds: $C_{10}HNO_3$.*

For all studied plates of GIC $C_{10}HNO_3$, the CESR spectrum, as in graphite, consists of a single line with the axial angular dependence relative to the ***c***- axis. The principal values of *g*-factor are equal to g_c=2.0023±0.0002 and g_a= 2.0028±0.0002. The value of A/B does not depend on *d* and *h*. The *A/B*(*l*) dependences in quasi-liquid ($T>T_c\approx$250 K) and in crystalline ($T<T_c$) phases of intercalate subsystem essentially differ from each other (Fig. 13). In a quasi-liquid phase of the intercalate this dependence has qualitatively the same form as the corresponding dependence in graphite, except for the small extremum for $l^*\approx$ 0.06 cm (Fig. 13a). This extremum is observed as well as in a solid phase of the intercalate, where at $l>l^*$ the *A/B*(*l*) dependence has an one-peak shape (Fig. 13b).

3.4 *Activated carbon fibers*.

The X-ray difractograms of the ACFs show very broad peaks at the graphite (002), (100) and (101) positions, where graphite (100) and (101) peaks merge into a single broad peak around 45^0.

In order to estimate the sizes *L* of the graphite nanoparticles in ACFs, the intensities of that were corrected for the Lorenz-polarization factor

$$LP(\theta)=(1+\cos^2 2\theta)/\sin^2\theta\cos\theta$$

The atomic form factor $f(\theta)$, and the factor

$$A(\theta)=\mu/2[1-\exp(-2\mu t/\sin\theta)],$$

where μ is the absorption coefficient and *t* is the thickness of the sample. The total correction of the intensities is then given by the equation

$$I_{corrected}=I_{obseved}/LP(\theta)\times f^2(\theta)\times A(\theta).$$

Using the corrected (002), (100) and (101) peak parameters we estimate the thickness and the in-plane size of the particle grains. From the broad graphite (002) peak, we find a grain thickness of $t\approx$2.1 nm. We deconvulate the broad feature around 43^0-47^0 into single (100) and (101) peaks on the assumption that each peak originates mostly from a single component. The obtained contribution to the (100) peak gives an estimate of the in-plane size of $L_a\approx$ 3 nm. From the location of peak centers for the c-axis diffraction (002) peak at 25.13^0 the interlayer distance between graphen sheets are estimated at 0.353 nm, which are considerably longer than the interlayer distance of 0.3354 nm for bulk regular graphite. From nanographite sample thickness and interlayer distance between graphene

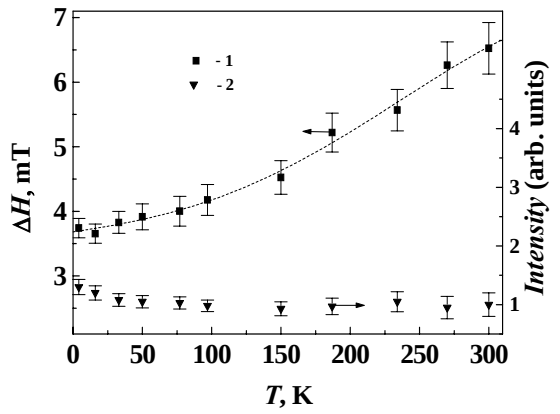

Fig. 14. Temperature dependence of the linewidth ΔH (1) and the intensity I (2) for the ESR signal in activated carbon fibers. The X-band. The lines are only a guide to the eye.

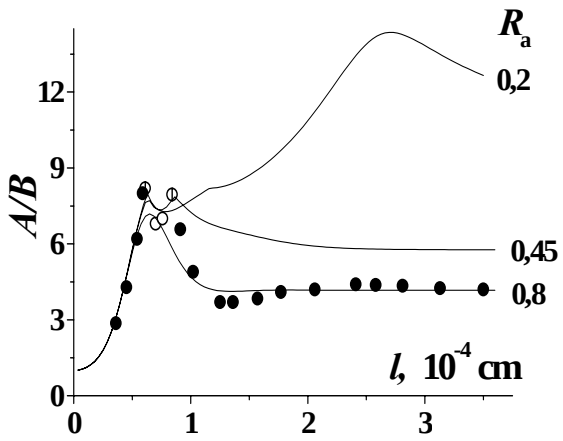

Fig. 15. Experimental (dots) and theoretical (lines) values of CESR lineshape asymmetry parameter, A/B, on sample thikness l. The theoretical curves were calculated using the Dyson [15] expressions for CESR lineshape without taking into account the effects of surface spin relaxation of current carriers. The shaded and open dots are referred to the 'normal' and 'reversed' lineshape, respectively; half-shaded dot corresponds to the lineshape with symmetric phase with respect to the A peak. $R_a=(T_{Da}/T_2)^{1/2}$ (T_{Da} is the time of spin diffusion across the skin-depth δ_c governed by the σ_c – conductivity, and T_2 is the intrinsic spin-relaxation time).

sheets, the number of graphene sheets are estimated at ~6.

The ESR spectrum of ACFs consists of a single line, which g-factor value is close to the g-factor value for free electron, and with the peak-to-peak width ~7.5 mT. The EPR signal is practically symmetric, that specifies a weak anisotropy of the g-factor. At lowering of the temperature the ESR signal is narrowed at near constant values of the g-factor and integral intensity (Fig. 14).

The intercalation of nanographite bloks in ACFs by nitric acid molecules was carried out as by exposition of ACFs in the intercalate atmosphere, and by the direct contact of ACFs with the liquid intercalate. In both cases the spectrum of the final nanographite intercalation compounds consists of a single symmetric line with the g-factor value being close to the free electron value and with the linewidth ~1 mT. At the decreasing of temperature, the linewidth of ESR signal increases at near constant value of the g-factor. At T_c~250 K the linewidth and the integral intensity of ESR signal are steeply increase.

The distance between graphen sheets in nanographites decreases at the adsorption by ACFs of water and some other molecules. Such compression of nanographites is accompanied by the change of g-factor and integral intensity of conduction ESR signal.

4. DISCUSSION

4.1 *Graphite*: *dependences of CESR lineshape and linewidth on sample size*

The dependences of CESR lineshape asymmetry parameter *A/B* and linewidth ΔH on graphite plate width (Figs. 4 and 5) essentially differ from the known theoretical curves, calculated from the Dyson [15] CESR lineshape expression without taking into account the effects of surface spin relaxation. First, the presence of l values, for which the CESR lineshape has an 'inverted' phase is a characteristic property of the theoretical curves $A/B(l)$ for the ratio $R_a=(T_{Da}/T_2)^{1/2}$ (where T_{Da} is the time of spin diffusion across the skin-depth δ_c governed by the σ_c – conductivity, and T_2 is the intrinsic spin-relaxation time) being less than 0,6 (Fig. 15), whereas the experimental values of *A/B* for $l >> \delta_c$ are consistent with the theoretical values of this parameter for $R_a>0.8$. Second, the values of *A/B* in the extrema of the experimental $A/B(l)$ dependence differ considerably from those for the theoretical curves (Fig. 15). Third, at $l\rightarrow 0$ the experimental values of CESR linewidth tends to the infinity (Fig. 5), whereas the corresponding Dyson [15] theoretical curve calculated from the Dyson [15] CESR lineshape expression without taking into account the effects of surface spin relaxation tends to the finite value, which differs from that for plates with $l >> \delta_c$ by 10% only (Fig. 5).

The character of CESR linewidth dependence on l (Fig. 5) uniquely specifies the presence of the contribution of surface spin relaxation into total spin relaxation of current carriers in HOPG plates investigated. Basing on this conclusion the above peculiarities of experimental results were analized in the framewoks of the extended Dyson theory [15] including the effects of surface spin relaxation of current carriers. In Figs. 4, 5 and 16 the results of theoretical calculations, respectively, of *A/B*, ΔH and lineshape dependences from sample width in the frameworks of the extended Dyson [15] theory are presented. (At calculation of the theoretical curve $A/B(l)$, the absorption of microwave field through all lateral surfaces both parallel and perpendicular to the ***c*** - axis was taking into account and the uniform distribution of microwave field near the vertical surfaces of the plates was supposed). From Figs. 4, 5 and 16 it can be seen that the theoretical curves with the non zero value value of Dyson [15] surface spin relaxation parameter $G_a=(3\varepsilon/4\Lambda_a)$ (ε is a probability of spin reorientation during the collision of current carriers with the surface and Λ_a is a mean free path of current carriers in a basal plane) describe the experimental data well.

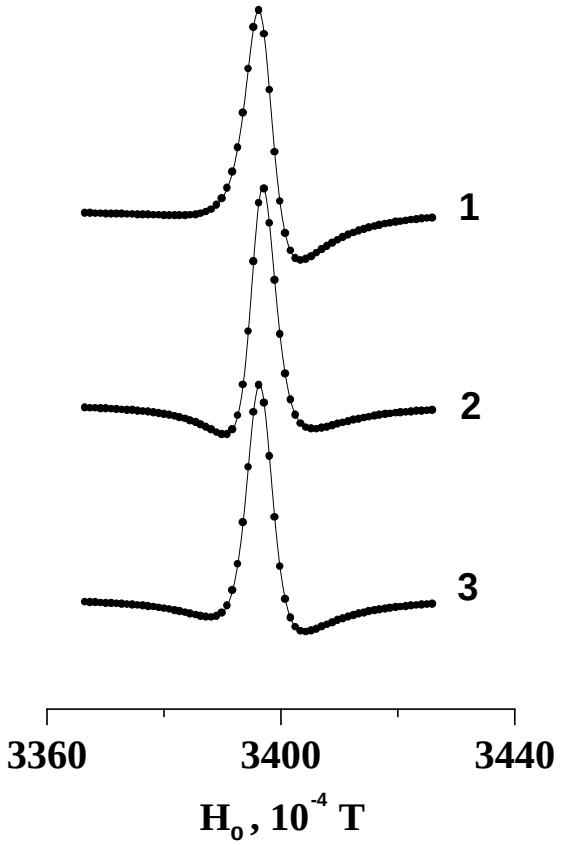

Fig. 16. A comparision of the experimental (solid lines) and theoretical lineshapes (points) for the first-derivative ESR absorption spectrum of graphite plates with dimensions l×0,355×0,075 cm^3. The theoretical curves were calculated from the Dyson [15] CESR lineshape equation with G_a=180 cm^{-1}, R_a=2.5 and T_2=1,3×10^{-8} s. The experimental spectra 1, 2 and 3, respectively refer to plates with l=0,26, 0,07, 0,054 cm. $\boldsymbol{c}\perp\boldsymbol{H}_0$, $\perp\boldsymbol{H}_{rf}$; ν=9,52 GHz, T=300 K.

4.2 *Graphite: the temperature dependence of CESR linewidth.*

The first systematic study of temperature dependences of graphite CESR signal parameters was carried out as early as 1960 by Wagoner [1] using a natural single crystal specimen in the temperature range from 77 K up to 600 K. After Wagoner a number of authors [2, 11-14] conducted similar studies on a variety of well-defined specimens of graphite, and have obtained nearly the same results. In particular, in all samples investigated and for all orientations of $\boldsymbol{H}_0$ relative to the $\boldsymbol{c}$-axis the graphite CESR signal linewidth increases first with decreasing temperature. According to the data of Matsubara *et al.* [14], the $\Delta H(T)$-dependence forms a distinct peak near 20 K and then falls off.

At present there is no consensus between researchers on both the graphite CESR linewidth and its temperature dependence origin. Kawamura *et al*. [13] showed that at $\boldsymbol{H}_0\|\boldsymbol{c}$ the Elliot's [22] expression for the CESR linewidth due to carriers interacting with phonons and/or impurities, which for $T>>\Theta_D$ (Θ_D is the Debye temperature) can be written as:

$$\Delta H_i = const\times(\Delta g_i)^2/\gamma m^*\mu(T) \quad (i=a, c) \qquad (1)$$

($\Delta g_i=g_i-g_0$ (i=a, c), where g_0 is the g-factor value for free electron, γ is the electronic gyromagnetic ratio, m^* is the carriers effective mass, and $\mu(T)$ is the carriers mobility), describes the graphite CESR linewidth in the interval 77÷300 K qualitatively at least. Matsubara *et al.* [14] considered the temperature variation of graphite CESR linewidth at $\boldsymbol{H}_0\|\boldsymbol{c}$ as a direct consequence of motional narrowing effect through an averaging process of g-values of scattered carriers over the Fermi surface in the limit of incomplete line averaging. In this limit the g-shift is averaged over all energy states of current carriers in $\boldsymbol{k}$-space, but the linewidth contains the components which are proportional to the square of the microwave frequency. Kotosonov [12] pointed out that the small ΔH values of the spectral lines suggest complete averaging of the g-factor over all the energy states of current carriers during the spin-lattice relaxation. Thus, for example, in synthetic graphite samples the temperature change from 40 K to 100 K leads to the g_c changing by ~0.2, which agrees with the resonance field shift by ~3×10^{-2} T, whereas the CESR linewidth remains within the limits of several oersteds.

According to the literature data [23, 24], in graphite the Debye temperature for longitutional acoustic out-of-plane modes is nearly 400 K. Therefore the description of the graphite CESR linewidth temperature dependence by Exp. (1), proposed by Elliot for $T>>\Theta_D$, is not obvios. Furthermore, this expression does not explain the presence of linewidth temperature dependence at $\boldsymbol{H}_0\perp\boldsymbol{c}$ (Fig. 6) even at a qualitative level since in this orientation of $\boldsymbol{H}_0$ the value of g_a does not depend on temperature (Fig. 7). The independence of the CESR linewidth on the microwave frequency shows that Matsubara's *et al.* [14] interpretation of the linewidth temperature dependence as a result of the motional narrowing of the incomplete averaging line is not correct also. Besides, the presence of low-temperature peak in $\Delta H(T)$ curve also at $\boldsymbol{H}_0\perp\boldsymbol{c}$, where g–factor is temperature independent, shows that the origins of low-temperature peaks in $g_c(T)$ and $\Delta H(T)$ dependences are different. The Kotosonov`s [12] point of view does not contradict to the experimental data, but he did not consider the nature of linewidth temperature dependence.

Above, it was pointed out that the characters of the $A/B(l)$ (Fig. 4) and $\Delta H(l)$ (Fig. 5) dependences of CESR line in graphite uniquely specifies the presence of the contribution of surface spin relaxation into total spin relaxation of current carriers in samples investigated. Basing on this fact, we considered the temperature dependence of CESR linewidth in HOPG also in the frameworks of model including surface spin relaxation effects of graphite π-electrons. Additionally, we suppose the presence of a small amount of the localized spins (~1% of the current carrier concentration or near one localized spin per 10^6 carbon atoms) and complete averaging of g-factors of the conduction electrons and localized spins. In such case, the CESR linewidth ΔH_i (i=a, c) can be presented in the following form:

$$\Delta H_i = \Delta H_{ie}^{surf}(\chi_e/\chi_e+\chi_s) + \Delta H_{ie}^{intr}(\chi_e/\chi_e+\chi_s)+ \\ +\Delta H_{is}(\chi_s/\chi_e+\chi_s) = F_1+F_2+F_3 \qquad (i = a, c), \qquad (2)$$

where ΔH_{ie}^{surf} and ΔH_{ie}^{intr} are the contributions to the total linewidth of conduction ESR signal due to interaction of conduction electrons with sample surface and inner imperfections, respectively; ΔH_{is} is the contribution to the

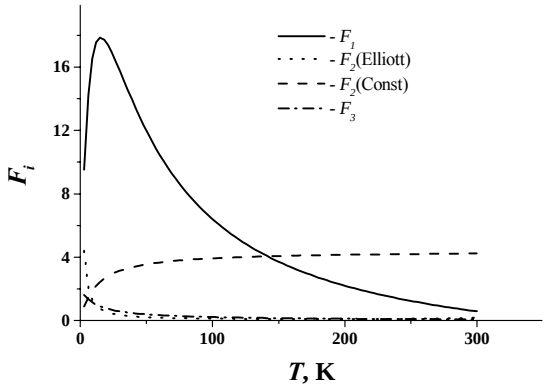

Fig. 17. The temperature dependences of F_i (i=1, 2, 3) (see Exp. (2)). The lines F_2(Elliott) and F_2(const) were calculated with the value of ΔH_{ie}^{intr} which changes on temperature according to the Elliot law (4) and not depend on temperature, respectively.

total linewidth due to the localized spins; χ_e and χ_s are the Curie and Pauli paramagnetic susceptibilities, respectively. At the calculations we assumed, that

$$\Delta H_{ie}^{surf} = a_{\mu i}\,\mu_{ai}(T) \qquad (i=a, c), \qquad (3)$$

where $a_{\mu i}$ is a constant depending on physical properties of a sample surface and orientation of $\boldsymbol{H}_o$ relative to the $\boldsymbol{c}$-axis. Because the Elliot`s expressions [22] for the intrinsic spin relaxation of current carriers were calculated for the simple isotropic metals, their applications to the graphite is not obvious. Therefore, the calculations of ΔH_i were carried out by us with values of ΔH_{ie}^{intr} both independent, and dependent on temperature according to the Elliot [22] law for $T<<\Theta_D$:

$$\Delta H_i = const\times(\Delta g_i)^2\Theta_D/\gamma m^*\mu_{ai}(T)\ T^2 \quad (i = a, c). \qquad (4)$$

Basing on the analysis of literature data on the temperature dependence of current carriers mobility in graphite basal plane [25] $\mu_{ai}(T)$ (i= a, c; this subindex was introduced for the account of dependence of carriers mobility on $\boldsymbol{H}_0$-orientation) was approximated by the following expression

$$\mu_{ai}(T) = a_i + b_i/(c_i+T)^{1.6} \quad (i = a, c),$$

where a_i, b_i and c_i are the varied parameters; at calculations of ΔH_i for $\boldsymbol{H}_0\perp\boldsymbol{c}$, their initial values were taken equal to –4 m^2/Vs, 63×10^3 $m^2\cdot K^{1.6}$/Vs and 55 K, respectively, for intrinsic linewidth temperature dependence determined by the Exp. (4) and were taken equal to –0.4 m^2/Vs, 13.25×10^3 $m^2\cdot K^{1.6}$/Vs and 24.5 K, respectively, for constant intrinsic linewidth (in both cases, for the chosen values of parameters the $\mu_{ac}(T)$-dependences approximately correspond to the in-plane mobility of carriers in the average on quality HOPG). Taking into consideration the data of irradiated graphite CESR-measurements [26] the values of g_s and ΔH_{is} were taken equal to 2,0023 and 0,25 mT, respectively. The values of $a_{\mu i}$ in Exp. (3) and constants in Exp. (4) were calculated using the literature data on the value of $\mu_{ai}(T)$ in HOPG [25] and surface and intrinsic spin relaxations times at room temperature extracted from the analysis of experimental $\Delta H(l)$ data (Fig. 5), respectively.

The results of approximation of experimental temperature dependence of CESR linewidth at $\boldsymbol{H}_0\perp\boldsymbol{c}$ by Exp. (2) are presented in Fig. 6. As it is seen from this figure, for both forms of temperature dependence of intrinsic spin relaxation rate the theoretical curve $\Delta H_i(T)$ contains the distinct peak near 20 K. At the same time, the theoretical analysis of Exp. (2) has shown (Fig. 17), that this peak is absent if $\Delta H_{ie}^{surf}=0$.

In the frameworks of the model considered in all temperature interval of investigations the best description of the experimental temperature dependence of CESR linewidth by Exp. (2) was achieved with temperature independent value of intrinsic spin relaxation rate (see Fig. 6). We believe that this fact has a physical sense and it is a consequence that in a real graphite the collisions of current carriers with the graphite crystallite boundaries introduce main contribution into intrinsic spin relaxation rate.

4.3 *Evolution of CESR lineshape and linewidth at graphite intercalation by HNO_3.*

With the configuration of our ESR experiment (Fig. 1) the microwave field penetrates into the HOPG plate mainly through its lateral sides, which are parallel to both the $\boldsymbol{c}$-axis and $\boldsymbol{H}_{rf}$ [11], i.e. through the lateral sides $h\times d$. Therefore, the evolution of graphite CESR signal of the sample investigated (Fig. 8) is mainly due to variations of the composition and properties of the HOPG plate at the surface areas from these sides. The dependence of the shape and intensity of graphite CESR signal on exposure time, τ, of a sample in HNO_3 vapours is qualitatively identical to that of the ESR signal lineshape and intensity of the localized spins in a metallic substrate on the thickness of a spray-coated film of another metal [27]. In our case, the spins in consideration are certainly mobile, but for $l/\delta_c<2$ the CESR line shape does not depend on spin mobility [9,11], i.e., in the framework of the Dyson theory [15] in HOPG plate investigated the spin carriers may be considered as localized. Therefore, the variations of the shape and intensity of the graphite CESR signal (Fig. 8) may be considered as being due to the formation of a macroscopic 'intercalation' layer on the HOPG plate (with conductivity being different from that of the initial material) and by advance of the interface separating this layer from as-yet the non-intercalated parts of sample (due to the diffusion of nitric acid molecules into the substrate along the graphite galleries). The invariability of the g-factor values for CESR signal from HOPG substrate (g_i) and that from 'intercalation' layer (g_i*) up to the disappearance of signal and the end of reaction, respectively, indicates that the interface between 'intercalation' layer and as-yet the non-intercalated parts of sample may be considered as non-conductive. The non-conductivity of this interface may be caused by significant distortion of a carbon net near the intercalation front and/or by the presence of high phase-boundary electrostatic potential due to the different current carriers concentration in the intercalated parts of graphite and in the non-intercalated ones.

In the experiment under consideration, the whole volume of sample investigated is available for CESR studies. Therefore, the time of the graphite CESR signal disappearance corresponds approximately to the moment of

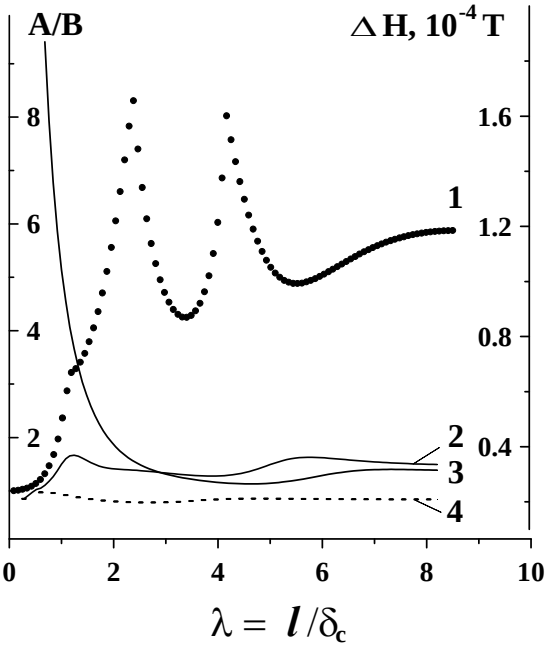

Fig. 18. Calculated CESR lineshape asymmetry parameter, *A/B* (1), and linewidth, ΔH (2), vs. $\lambda = l/\delta_c$. in GIC $C_{10}HNO_3$. at $T>T_c$ for the case of simulteneously presence in sample of localized spins and surface spin relaxation of current carriers. The curves 3 and 4 correspond to $\Delta H(\lambda)$ dependences for conduction electrons and localized spins, respectively. The X-band.

contact of the counter (antiparallel) intercalation fronts. Let us assume, that the intercalation is determined by a two-dimensional diffusion-controlled process, i.e. the thickness of the intercalated layer, d^*, depends on the exposure time as $(d^*)^2=2D_{int}\times\tau$, where D_{int} is intercalate two-dimensional diffusion constant. In such a case, having substituted the value of time interval from the beginning of the graphite CESR signal transformation up to its disappearance, $\tau\cong3$ h, and $d^*=l/2$ to this expression, it is easy to estimate the value $D_{int}\sim2\times10^{-12}$ m^2 s^{-1}. It is worth to note that this value of D_{int} well correlates with that obtained by high-resolution neutron scattering by Simon *et al*. [28]: $D_{int}\cong4\times10^{-12}$ m^2 s^{-1}.

A new and unexpected result of this experiment is the significant broadening of the graphite CESR signal from the beginning of the intercalation up to the contact of the counter intercalation fronts (Figs. 8 and 10). We suppose that the reason for it is the collisions of current carriers (at their diffusion along the graphite layers) with the non-conductive interface between the intercalated and the non-intercalated parts of the HOPG plate. Indeed, when the intercalation front advances into the HOPG plate (due to the diffusion of nitric acid molecules into the graphite along the graphite galleries) the width of its non-intercalated part decreases and, therefore, the frequency of collisions of graphite current carriers with these interfaces increases. Therefore, assuming the probability of spin reorientation of graphite current carriers during such collisions to be non-zero, the increase of the total rate of spin relaxation of graphite current carriers (the graphite CESR linewidth) with the time of intercalation can be observed. Note, that in all previous ESR experiments on graphite intercalation [4-9] which were carried out on HOPG plates with $l>>\delta_c$, no broadening of the graphite CESR signal was observed. This indirectly supports our interpretation of the graphite CESR signal broadening at the intercalation of the narrow ($l\sim2\delta_c$) HOPG plate.

The increase of $A^*/B^*(\tau)$ dependence at the beginning of intercalation from 1 until 3.7 (Fig. 12) corresponds to a theoretical $A/B(\lambda)$-dependence changing when increasing λ (λ is the ratio of a sample thickness to the skin-depth) [9, 11]. At the constant value of electrical conductivity along the ***c***-axis of the forming GIC stage, this fact also points to the presence of the non-conductive barrier through the intercalation front and on its advance into sample. Under such understanding of the nature of $A^*/B^*(\lambda)$-dependence (Fig. 12) a changing of the skin-depth governed by the ***c***-axis conductivity of GICs from the beginning to the end of reaction may be easily determined by using the maximum and minimum values of A^*/B^* and the well known $A/B(\lambda)$ -nomograms for different *R*-values [9, 11]. Such kinds of calculations show that the skin-depths of the initial 7-th stage and of the final 2-d stage of GICs differ approximately in 1.6 times.

Using the relation $(d^*)^2=2D_{int}\times\tau$ the experimental dependence $\Delta H(\tau)$ can be easily transformed into the dependence $\Delta H(a)$, where $a = l-2d^*$ is the thickness of the non-intercalated part of HOPG plate (Fig. 10). The latter dependence can be calculated theoretically as well, using the exdended Dyson expressions for the CESR in metals including the effects of surface spin relaxation [15]. (The analysis of the mentioned Dyson expression has shown that at given sample thickness the CESR linewidth increases with *G* value. For $G\neq0$, the value of CESR linewidth tends to the infinity at $\theta\rightarrow0$). Obviously, if $\varepsilon\equiv\varepsilon_a$ is considered as an average value of probability of spin reorientation during collisions of graphite current carriers with the non-conductive phase boundary, then the extended Dyson expressions for the CESR in metals including the effects of surface spin relaxation of current carriers can be used for analysis of $\Delta H(a)$ dependence also. It is shown in Fig. 10, where the results of such analysis are presented, that the theoretical dependence of the graphite CESR linewidth, with non-zero values of G_a describes the experimental data well. The found value of G_a=1 [10] cm^{-1} and the typical HOPG values of $\Lambda\equiv\Lambda_a=(0.4\div1.6)\times10^{-5}$ cm [33] correspond to $\varepsilon_a=(0.5\div2.1)\times10^{-4}$ [$(0.5\div2.1)\times10^{-3}$]. It is worth noticing that at present there are no data on interface spin relaxation in conductors in literature. There are only some published data on surface spin relaxation in simple metals. For comparison, the surface spin reorientation probabilities of conduction electrons in Cu and Li bulk samples are equal to $\sim10^{-2}$ [34] and $\sim5\times10^{-6}$ [35], respectively.

It is obvious, that the spins of current carriers colliding with the front of reaction from the intercalated part of graphite also have some probability of reorientation, ε_a^*, during such collisions. Therefore, the analysis of $\Delta H^*(\tau)$-dependence (Fig. 11) it is possible to execute on the same procedure, which above was used for the analysis of the $\Delta H(\tau)$-dependence (Fig. 10). The application of the specified technique of the analysis to the experimental $\Delta H^*(\tau)$-dependences (Fig. 11) give the G_a^*-values: ~180 cm^{-1} in one experiment and ~70 cm^{-1} in the other experiment. As we see, both values of G_a^* appreciably greater than the values of G_a. If $\varepsilon_a=\varepsilon_a^*$, it means that already in the GIC stage originally forming the mean free path of current carriers in a basal plane appreciably shooter, than in initial graphite.

4.4 *Graphite inercalation compounds* ($C_{10}HNO_3$): *CESR lineshape dependence on sample sizes.*

The analysis had shown that the theoretical curves *A/B*(*l*) have an weak extremum (from the direction of smaller *l*) only under the simultaneous contribution to the ESR spectrum of the next two factors: 1) the surface spin relaxation of current carriers and 2) a small amount of the localized spins with the value of *g* – factor being nearly equal to that for conduction electrons but which spin-states are not average with spin-states of the conduction electrons. As seen from Fig. 18, the coordinates of first extremums of the *A/B*(λ)- and $\Delta H(\lambda)$-dependences approximately coincide.

The presence a weak extremum at *l** in the experimental *A/B*(*l*) dependence for the $C_{10}HNO_3$ plates (Fig. 13) testifies that both the surface spin relaxation and localized spins make a contribution to the ESR signal of GICs investigated. In the frameworks of this model we have been able to describe the experimental *A/B*(*l*) dependence well above [below] T_c with the next set of parameters: G_a=23 cm^{-1} [(5.4+270·*exp*(-*l*/l_0)) cm^{-1}, where l_0=0.025 cm], N_s/N_e (the ratio of intensity of ESR signals of the localized and the delocalized spins)=0.15 (0.3), T_{2s}/T_{2e} (the ratio of spin-lattice relaxation times for the localized and the delocalized spins)=0.75 (1) and $\Delta g_{s\text{-}e}$ (the difference in *g* – values of the localized and delocalized spins)=6 (6)×10^{-5} (Fig. 13). It is worth to note that the change of ratio N_s/N_e at the aggregate phase transition in the intercalate subsystem follows from above calculations.

4.5 *Activated carbon fibers*.

The EPR experimental data for nanographite bloks in ACFs are near similar to that for nanographites obtained by heat treatment of diomond [36]. Reduction of the value and the anisotropy of g-factor in nanographite in comparison with the bulk graphite specify smaller value of the spin-orbit interaction for conduction electrons in nanographite. The most probable reason for this is the increase of intersheet distance in nanographites, resulting to the reduction of overlapping of conducting and valent π-zones. The value of ESR linewidth in nanographite on the order is more, than in bulk regular graphite. This fact contradicts to the well-known Elliott [22] theory of spin-lattice relaxation in bulk regular conductors, according to which the conduction ESR linewidth is proportional $(g-g_0)^2$. At the same time the specified result may be explained in the frameworks of the author's model for the conduction electron spin-relaxation in carbon materials (see Chapter 4.1). In particular, according to this model in graphite an essential contribution of surface spin relaxation into the total spin relaxation rate is present.

Note, that despite of an vicinity of $|g-g_0|$ values in nanographites and in their intercalation compounds with nitric acid the ESR signal in the former is much wider, than in the latter. Possible reason of this is the destruction of the edge-located magnetic states [37] of nanographites at their intercalation by nitric acid molecules.

5. CONCLUSIONS

In graphite and its intercalation compounds the influence of sample size and experimental conditions on CESR signal lineshape and linewidth had been studied. The analysis of experimental results uniquely points to the presence of large contribution of surface spin relaxation effects into the total rate of spin relaxation (i.e. into the CESR linewidth) of current carriers in samples investigated. In nanographite blocks of ACF the surface spin relaxation effects give the main contribution into the spin relaxation rate of current carriers.

As a results of an *in situ* conduction CESR studies of HNO_3 molecules intercalation into narrow HOPG slab, the contribution of collisions of the graphite and GIC current carriers with the graphite intercalation front into their total spin relaxation rate had been revealled. Under the assumption that the graphite CESR signal evolution is caused by the advance of a boundary separating the intercalated and non-intercalated sample the average probability value of spin reorientation during the collision of current carriers with this interface and the constant of two-dimensional diffusion of nitric acid molecules into HOPG have been extracted from experimental data.

The theoretical analysis had shown that the curves A/B(*l*) have an weak extremum (from the direction of smaller *l*) only under the simultaneous contribution to the ESR spectrum of the next two factors: 1) the surface spin relaxation of current carriers and 2) a small amount of the localized spins with the value of g – factor being nearly equal to that for conduction electrons. In $C_{10}HNO_3$ plates the presence of a weak extremum in the experimental A/B(*l*) dependence at the small values of *l* (Fig. 13) testifies that both these factors make a contribution into the ESR signal. In the frameworks of this model we have been able to describe the experimental A/B(*l*) dependences well both above, and lower T_c.

Basing on the obtained results it may be supposed that many of existing problems connected with application of CESR technique to the study of graphite, GICs and other conducting carbon materials will be successfully solved after introducing into the consideration of surface and interface spin relaxation effects. The works in this direction are in progress.

ACKNOWLEDGMENTS

The author is grateful to N.M. Mishchenko, V.V. Kainara, A.N. Krivoshei P.G. Skrylnik for help in experiments and calculations and to L.B. Nepomnyashchii (Scientific Research Centre for Graphite, Moscow) for providing the HOPG. This work was supported by the Russian Foundation for Basic Research (grant No. 00-03-32610).

References

[1] Wagoner G. Spin Resonance of Charge Carriers in Graphite. Phys. Rev. 1960;118(3):647-653.

[2] Singer LS, Wagoner G. J. Electron spin resonance in polycrystalline graphite. Chem. Phys. 1962; 37(8):1812-1817.

[3] Khanna SK, Falardeau ER, Heeger AJ, Fischer JE. Conduction electron spin resonance in acceptor-type graphite intetcalation compounds. Solid State Commun. 1978; 25:1059-1065.

[4] Lauginie P, Estrade H, Conard J, Guerard D, Lagrange P, Makrini MEl. Graphite lamellar compounds EPR studies. Phisica B (Utrecht) 1980; 99:514-520.

[5] Davidov R, Milo O, Palchan I, Selig H. ESR study of graphite-fluorine and graphite-fluoride acceptor intercalation compounds. Synth. Met. 1983; 8:83-87.

[6] Palchan I, Davidov D, Zevin V, Polatsek G, Selig H. An in situ ESR study of the intercalation

mechanisms: HOPG/fluorine and HOPG/HNO_3. Synth. Met. 1985; 12:413-418.

[7] Stein RM, Wamsley L, Rettori C. Temperature dependence of the electrical resistivities in $AlCl_3$-graphite intercalation compounds determined by conduction-carrier spin resonance. Phys. Rev. 1985; B32:4134-4142.

[8] Saint Jean M, Rigaux C, Clerjaud B, Blinowski J, Kacman P, Furdin G. Electron spin resonance in graphite acceptor compounds. Ann. Phys. (Paris) 1986; 11:215-227.

[9] Saint Jean M, McRae EP. Planar diffusion constant D_a in acceptor-graphite intercalation compounds. Phys. Rev. 1991; B43: 3969-3974.

[10] Ziatdinov AM, Mishchenko NM, Nikolenko YuM. Phase transitions and incommensurate states in GIC $C_{5n}HNO_3$. Synth. Met. 1993; 59:253-258.

[11] Ziatdinov AM, Mishchenko NM. Electron spin resonance lineshape and kinetic parameters of the conduction electrons in highly anisotropic conductors: highly oriented pyrolitic graphite. Phys. Solid State 1994; 36(8):1283-1289.

[12] Kotosonov AS. *g*-factor of current carriers in pyrolytic carbons with quasi-two-dimensional graphite structure. Carbon 1988; 26(2):189-195.

[13] Kawamura K, Kaneko S, and Tsuzuku T. Conduction electron spin resonance of graphite. J. Phys. Soc. Jpn. 1983; 52(11):3936-3942.

[14] Matsubara K, Tsudzuku T, Sugihara K. Electron spin resonance in graphite. Phys. Rev. 1991; B44:11845-11851.

[15] Dyson FJ. Electron spin resonance absorption in metals. II. Theory of electron diffusion and the skin effect. Phys. Rev. 1955; 98(2):349-359.

[16] Kaplan JI. Application of the diffusion-modified Bloch equation to electron spin resonance in ordinary and ferromagnetic metals. Phys. Rev. 1959; 115(3):575-577.

[17] Feher G, Kip AF. Electron spin resonance absorption in metals. I. Experimental. Phys. Rev. 1955; 98(2):337-348.

[18] Kodera HJ. Dyson effect in the electron spin resonance of phosphorus doped silicon. Phys. Soc. Jpn. 1970; 28(1):89-98.

[19] Pifer JH, Magno R. Conduction electron spin resonance in a lithium film. Phys. Rev. 1971; B3(3):663-673.

[20] Müller KA, Berlinger W, Pfluger P, Geiser V, Güntherodt HJ. Transition from three to a near two-dimensional metallic state in C_6Li. Solid State Comm. 1985; 55(9): 803-806.

[21] Blinowski J, Kacman P, Rigaux C, and Saint Jean M. Effect of conduction anisotropy of GIC on ESR line shape. Synth. Met. 1985; 12:419-423.

[22] Elliot RJ. Theory of the effect of spin-orbit coupling on magnetic resonance in some semiconductors. Phys. Rev. 1954; 96(2):266-279.

[23] Gschneider KA. Specific-heats of graphite intercalation compounds. Solid State Physics 1964; 16(4):275-282.

[24] Mizutani U, Kondow T, Massalski TB. Low temperature specific-heats of graphite intercalation compounds with potassium and cesium. Phys. Rev. 1978; B17(8):3165-3173.

[25] Dresselhaus MS, Dresselhaus G. Intercalation compounds of graphite. Adv. Phys. 1981; 30(2):139-326.

[26] Miyake M, Saiki W, Daimon T, Son P, Miyake C, Ohya-Nishiguchi H. ESR spectra in graphite irradiated with He^+ ions. J. Nucl. Mat. 1992; 187:138-145.

[27] Zevin V, Suss JT. ESR in layer-substrate structures: The line shape and nondestructive contactless measurements of the layer conductivity. Phys. Rev. 1986; B34(10):7260-7270.

[28] Simon C, Rosenman I, Batallan F, Rogerie J, Legrand JF, Magerl A, Lartigue C, Fuzellier H. Measurement of defect mobility in a defect-mediated melting. Phys. Rev. 1990; B41(4):2390-2397.

[29] Palchan I, Mustachi F, Davidov D, Selig H. ESR study of dulate intercalation compounds: C/F, C/K/F and C/Li/F. Synth. Met. 1984/85; 10:101-106.

[30] Nakajima M, Kawamura K, Tsuzuku T. ESR study of HNO_3 intercalation process of graphite. J. Phys. Soc. Jpn. 1988; 57(5):1572-1575.

[31] Ziatdinov AM, Tsvetnikov AK, Mishchenko NM, Sereda VV. In situ ESR studies of intercalation of SbF_5 molecules into highly oriented pyrolitic graphite. Mat. Sci. Forum (Intercalation Compounds ISIC-6) 1992; 91-93:583-588.

[32] Ziatdinov AM, Mishchenko NM. In situ ESR study of the HNO_3-intercalate diffusion process in graphite intercalation compounds. J. Phys. Chem. Solids 1997; 58(7):1167-1172.

[33] Spain IL. Electronic transport properties of graphite, carbons, and related materials. Walker PL, Throweer Jr and PA, editors. Chemistry and physics of carbon, vol 8, New York:Dekker, 1973:119-305.

[34] Walker MB. Surface relaxation and quasiparticle interactions in conduction-electron spin resonance. Phys. Rev. 1971; B3(1):30-41.

[35] Zhikharev VA, Kessel AR, Kharakhashian EG, Cherkasov FG, Svarts KK. Conduction Electrons spin echo in metals. Soviet Phys.- JETP 1973; 64(4):1356-1366.

[36] Anderson OE, Prasad BLV, Sato H, Enoki T, Hishiyama Y, Kaburagi Y, Yoshikawa M, Bandow S. Structure and electronic properties of graphite nanoparticles. Phys. Rev. 1998; B58(24):16387-16395.

[37] Nakada K, Fujita M, Dresselhaus G, and Dresselhaus MS. Edge state in graphene ribbons: Nanometric size effect and edge shape dependence. Phys. Rev. 1996; B54(24):17954-17961.